



Contents lists available at ScienceDirect

## Journal of Quantitative Spectroscopy &amp; Radiative Transfer

journal homepage: [www.elsevier.com/locate/jqsrt](http://www.elsevier.com/locate/jqsrt)

# Comparisons of radiative transfer schemes for infrared spectra and the region with solar and infrared spectra overlap in RRTMG



Han Lin, Kun Wu\*, Wenwen Li

Key Laboratory of Meteorological Disaster, Ministry of Education/ Collaborative Innovation Center on Forecast and Evaluation of Meteorological Disaster, Nanjing University of Information Science and Technology, Nanjing, China

## ARTICLE INFO

## Article history:

Received 17 August 2019  
 Revised 29 December 2019  
 Accepted 13 January 2020  
 Available online 14 January 2020

## Keywords:

Radiative transfer  
 Overlap region  
 RRTMG  
 Large-sample test

## ABSTRACT

Five radiative transfer schemes are compared in infrared spectra using the Rapid Radiative Transfer Model for General Circulation Models Applications (RRTMG). By calculating the root mean squared error of net flux (referred as RMSE(NF)) in various atmosphere, the general accuracy of these schemes ranked from low to high are: non-scattering simplification (NS), the adding method of  $\delta$ -two-stream discrete ordinate approximation ( $\delta$ -2DDA),  $\delta$ -two-stream variational iteration method ( $\delta$ -2VIM), the adding method of  $\delta$ -four-stream discrete ordinate approximation ( $\delta$ -4DDA) and  $\delta$ -four-stream variational iteration method ( $\delta$ -4VIM). And their sensitivities to cloud fraction are decreased in the same order. Furthermore, the accuracy and efficiency of these schemes other than NS are studied under the contexts of using two different methods for dealing with the region where the solar and infrared spectra overlap. As one of the two overlap methods, One Band method (OB), which is used by RRTMG, has no advantage in model efficiency and is about 0.34 (0.41) W/m<sup>2</sup> higher in mean column RMSE(NF) of the  $\delta$ -two-stream ( $\delta$ -four-stream) schemes than Whole Bands method (WB). Moreover, a new scheme, which is simple but adequate to handle the overlap region, is derived to solve the solar energy in longwave spectra.

© 2020 The Authors. Published by Elsevier Ltd.

This is an open access article under the CC BY-NC-ND license.  
[\(http://creativecommons.org/licenses/by-nc-nd/4.0/\)](http://creativecommons.org/licenses/by-nc-nd/4.0/)

## 1. Introduction

Since radiation is the major energy source and sink in the atmosphere, an accurate treatment of radiative transfer equation (RTE) is necessary for general circulation models (GCMs). In the meanwhile, as one of the most time-consuming parts of GCMs, the RTE schemes also demand high efficiency. Therefore, approximate treatments for RTE have been extensively studied [e.g. [1–22,40]].

For solar radiative transfer (SRT), Lin et al. [23] compared five  $\delta$ -two-stream and  $\delta$ -four-stream schemes and concluded that the adding method of  $\delta$ -four-stream discrete ordinate approximation ( $\delta$ -4DDA; 16) and adding method of  $\delta$ -four-stream spherical harmonic expansion ( $\delta$ -4SDA; 17) are about an order of magnitude less in errors than the  $\delta$ -two-stream schemes, and respectively expend 1.76 and 1.55 times of running time consumed by the radiation model of  $\delta$ -two-stream schemes.

For terrestrial radiative transfer (TRT), the scattering is often neglected since scattering is strong in shortwave spectra but weak

in the longwave region [24]. However, such neglect can produce the near-global (60°S–90°N) reduction of 3 W/m<sup>2</sup> in the outgoing LW radiation due to cloud scattering reported by Costa and Shine [25], which amounts to 10% of the global LW cloud radiative effect at the top of the atmosphere (TOA) [26]. To refine the TRT scattering accuracy, a few schemes were developed in recent five years. Firstly,  $\delta$ -4DDA and  $\delta$ -4SDA have been expanded for TRT by Zhang et al. [27] and Wu et al. [28]. By comparing  $\delta$ -4DDA,  $\delta$ -4SDA and the adding method of  $\delta$ -two-stream discrete ordinate approximation ( $\delta$ -2DDA), Wu et al. [28] shows that the accuracy of both  $\delta$ -4DDA and  $\delta$ -4SDA is superior to that of  $\delta$ -2DDA, while  $\delta$ -4DDA is slightly more accurate than  $\delta$ -4SDA. Thereafter, Zhang et al. [20] introduced variational iteration method (VIM) to solve the RTE and obtained the  $\delta$ -two-stream solution ( $\delta$ -2VIM) and  $\delta$ -four-stream solution ( $\delta$ -4VIM). Moreover, Wang [19,29] presented a unified formulation for radiative transfer and derived hemispherical harmonics method with four components, which is comparable to  $\delta$ -4DDA in accuracy and can be applied to both solar and terrestrial radiation.

To make the code of RTE solution more efficient, the solar solutions are usually neglected in longwave region. Taking a widely-used radiation model so called Rapid Radiative Transfer Model for

\* Corresponding author.

E-mail address: [wukun@nuist.edu.cn](mailto:wukun@nuist.edu.cn) (K. Wu).URL: <http://cas.nuist.edu.cn/Teacher.aspx?T=003118> (K. Wu)

General Circulation Models Applications (RRTMG; 30) as an example, a scheme which neglects scattering and solar irradiance (NS) is applied in RRTMG\_LW (longwave part of RRTMG) while a  $\delta$ -two-stream scheme is used by default in RRTMG\_SW (shortwave part of RRTMG). However, there is still about 13.23 W/m<sup>2</sup> solar irradiance between 100 to 2600 cm<sup>-1</sup> within infrared region according to a solar irradiance dataset based on the Naval Research Laboratory Solar Spectral irradiance (NRLSSI2) model [31,32]. This part of solar irradiance can be treated as another band in SRT (referred as One Band method; OB) as RRTMG\_SW does. As for Whole Bands method (WB), since the radiative transfer process is governed by a linear equation, the total radiation of each longwave band should be the sum of the solar and terrestrial radiation [33]. The accuracy of these two methods has been compared in Zhang et al. [33] by single-column experiment in ideal atmosphere.

Although many TRT schemes and schemes with different overlap methods have been compared [e.g. [11,17,20,27,29]], there was little attention has been paid to the huge size requirement of profile samples to represent the complexity of atmosphere. In addition, although RRTMG is a widely-used radiation model, its performance with different TRT schemes and the schemes using different overlap methods has not been investigated yet.

Within this paper, five TRT schemes (NS,  $\delta$ -2DDA,  $\delta$ -2VIM,  $\delta$ -4DDA and  $\delta$ -4VIM) and the  $\delta$ -two/four-stream schemes ( $\delta$ -2DDA,  $\delta$ -2VIM,  $\delta$ -4DDA and  $\delta$ -4VIM) using two overlap methods (WB and OB) are generally compared with focus on their possible behaviors in realistic applications. In the following Section 2, a simple new scheme is derived to cope with the SRT in longwave region. The single column results are compared in Section 3, for terrestrial schemes and those with different overlap treatments in Section 4 and 3.2 respectively. The layout in Section 4 is like that of Section 3 but for large-sample results. An efficiency comparison of terrestrial schemes and those using different overlap methods is given in Section 5. Finally, summary and conclusions are presented in Section 6.

## 2. RTE solution of the overlap region

When dealing with the region with solar and infrared spectra overlap, a scheme that can handle the solar irradiance is required. Like  $\delta$ -2DDA and  $\delta$ -4DDA, both have their solar counterparts. As for VIM, however, because absorption approximation (AA; 34) is not suitable for SRT, the VIM which uses AA as an initial solution is not either. Therefore, a new simple scheme is established to cope with SRT of the overlap region in this section. This scheme is designed to be an efficient scheme that can keep adequate accuracy, and only used with VIM schemes in this work.

The solar RTE for diffuse intensity  $I(\tau, \mu)$  is [e.g. 1]

$$\mu \frac{dI(\tau, \mu)}{d\tau} = I(\tau, \mu) - \frac{\omega}{2} \int_{-1}^1 I(\tau, \mu') P(\mu, \mu') d\mu' - \frac{\omega}{4\pi} F_0 \exp\left(-\frac{\tau}{\mu_0}\right) P(\mu, -\mu_0), \quad (1)$$

where  $\tau$  and  $\omega$  are optical depth and single scattering albedo; the cosine of local emergence angle, local incident angle and solar zenith angle are marked as  $\mu$ ,  $\mu'$  and  $\mu_0$  respectively;  $P$  and  $F_0$  represent the azimuth-independent phase function and downward solar flux at the TOA.

For the overlap band, relatively, absorption is more significant than scattering. Thus, an approach which is enlightened from AA is taken to solve the solution of downward solar flux. The solar scattering process is simplified and the RTE becomes

$$\mu \frac{dI^0(\tau, \mu)}{d\tau} = (1 - \omega)I^0(\tau, \mu) - \frac{\omega}{4\pi} F_0 \exp\left(-\frac{\tau}{\mu_0}\right) P(\mu, \mu_0). \quad (2)$$

The solution of Eq. (2) is

$$I^0(\tau, \mu) = I^0(\tau_s, \mu) \exp\left[\frac{(1 - \omega)(\tau - \tau_s)}{\mu}\right] + \frac{F_0 \omega \mu_0 P(\mu, -\mu_0)}{4\pi [\mu_0(1 - \omega) + \mu]} \left\{ \exp\left(-\frac{\tau}{\mu_0}\right) - \exp\left[\frac{(1 - \omega)(\tau - \tau_s)}{\mu} - \frac{\tau_s}{\mu_0}\right] \right\}. \quad (3)$$

When calculating the downward path,  $\tau_s = 0$  is the initial point of optical depth and the value of  $\mu$  shall be negative. The downward intensity at  $\tau = \tau_1$  is

$$I^0(\tau_1, \mu) = I^0(0, \mu) \exp\left[\frac{(1 - \omega)\tau_1}{\mu}\right] + \frac{F_0 \omega \mu_0 P(\mu, -\mu_0)}{4\pi [\mu_0(1 - \omega) + \mu]} \times \left\{ \exp\left(-\frac{\tau_1}{\mu_0}\right) - \exp\left[\frac{(1 - \omega)\tau_1}{\mu}\right] \right\}. \quad (4)$$

In the conditions that  $\tau_s = \tau_1$ ,  $\tau = 0$  and  $\mu > 0$ , upward intensity  $I^0(0, \mu)$  can be obtained:

$$I^0(0, \mu) = I^0(\tau_1, \mu) \exp\left[\frac{(\omega - 1)\tau_1}{\mu}\right] + \frac{F_0 \omega \mu_0 P(\mu, -\mu_0)}{4\pi [\mu_0(1 - \omega) + \mu]} \left\{ \exp\left(-\frac{\tau_1}{\mu_0}\right) - \exp\left[\frac{(\omega - 1)\tau_1}{\mu} - \frac{\tau_1}{\mu_0}\right] \right\}. \quad (5)$$

So far a pair of SRT solutions (Eqs. (4) and (5)) is derived, but within which the upward implementation (Eq. (5)) will result in significant underestimation of upward flux at the TOA (results not shown). Hence, another scheme of upward path, which is enlightened from the two-stream source function technique [4,11], is established to mitigate that underestimation.

First of all, Eq. (1) is rewritten as:

$$\mu \frac{dI^1(\tau, \mu)}{d\tau} = I^1(\tau, \mu) - \frac{\omega}{2} \int_{-1}^1 I^1(\tau, \mu') P(\mu, \mu') d\mu' - \frac{\omega}{4\pi} F_0 \exp\left(-\frac{\tau}{\mu_0}\right) P(\mu, -\mu_0). \quad (6)$$

In the  $\delta$ -two-stream case,  $\int_{-1}^1 I^1(\tau, \mu') P(\mu, \mu') d\mu'$  in Eq. (6) is simplified as  $(1 + 3g\mu\mu_1)I^1(\tau, \mu_1) + (1 + 3g\mu\mu_{-1})I^1(\tau, \mu_{-1})$ , where  $g$  is asymmetry factor,  $\mu_1 = -\mu_{-1} = 1/1.66$  is diffuse factor (Elsasser 1942) and  $I^1(\tau, \mu_{-1})$  is substituted by  $I^0(\tau, \mu_{-1})$  from Eq. (4). As an upward path scheme, only  $\tau_s = \tau_1$ ,  $\tau = 0$  and  $\mu > 0$  are considered. The eventually obtained solution of  $I^1(0, \mu_1)$  is

$$I^1(0, \mu_1) = I^1(\tau_1, \mu_1) b + \frac{c(1 - 3g\mu_1\mu_0)}{f\mu_0\mu_1} \left[ \frac{b}{\exp(\tau_1/\mu_0) - 1} \right] + \frac{\omega\phi(\mu_1, \mu_{-1})}{2\mu_1} \left\{ I^0(0, \mu_{-1}) \frac{\exp(d\tau_1) - 1}{d} - \frac{c(1 - 3g\mu_{-1}\mu_0)}{\mu_0(\omega - 1) - \mu_{-1}} \left[ \frac{\exp(f\tau_1) - 1}{f} - \frac{\exp(d\tau_1) - 1}{d} \right] \right\}, \quad (7)$$

where

$$b = \exp\{\tau_1[\omega\phi(\mu_1, \mu_1) - 2]/(2\mu_1)\}, \\ c = \omega F_0 \mu_0 / (4\pi), \\ d = [2\omega + \omega\phi(\mu_1, \mu_1) - 4]/(2\mu_1), \\ f = \{\mu_0[\omega\phi(\mu_1, \mu_1) - 2] - 2\mu_1\}/(2\mu_0\mu_1), \\ \phi(\mu_i, \mu_j) = 1 + 3g\mu_i\mu_j \quad (i, j = \pm 1)$$

and the value of  $I^0(0, \mu_{-1})$  can be calculated by Eq. (4).  $I^1(\tau_1, \mu_1)$  in the first term of the right hand side of Eq. (7) is the boundary input calculated from the previous layer. Finally, the upward and downward fluxes become

$$F^\uparrow(0) = \pi I^1(0, \mu_1) \quad \text{and} \quad (8a)$$

$$F^\downarrow(\tau_1) = \pi I^0(\tau_1, \mu_{-1}) + \mu_0 \exp\left(-\frac{\tau_1}{\mu_0}\right) F_0. \quad (8b)$$

This  $\delta$ -two-stream scheme is named as Hemispherical source function approximation ( $\delta$ -2HSF).

In the  $\delta$ -four-stream case, two-node Gaussian quadrature is adopted to decompose the integration in RTE [35]:

$$\int_{-1}^1 I^1(\tau, \mu') P(\mu, \mu') d\mu' = \sum_{i=-2}^{i=2} a_i (1 + 3g\mu_i\mu) I^1(\tau, \mu_i) \quad (9)$$

in which  $\mu_1 = -\mu_{-1} = 0.2113248$ ,  $\mu_2 = -\mu_{-2} = 0.7886752$  and  $a_i = a_{-i} = 0.5$  ( $i = 1, 2$ ) [35,36]. The downward solutions ( $I^0(\tau_1, \mu_{-1})$  and  $I^0(\tau_1, \mu_{-2})$ ) can be calculated by replacing  $\mu$  with  $\mu_{-1}$  and  $\mu_{-2}$  respectively in Eq. (4). And by substituting  $I^0(\tau_1, \mu_2) \rightarrow I^1(\tau_1, \mu_2)$ ,  $I^0(\tau_1, \mu_{-1}) \rightarrow I^1(\tau_1, \mu_{-1})$  and  $I^0(\tau_1, \mu_{-2}) \rightarrow I^1(\tau_1, \mu_{-2})$  from Eqs. (4) and (5) into Eq. (9) and then into Eq. (6), intensities of upward path  $I^1(0, \mu_1)$  can be derived out as:

$$\begin{aligned} I^1(0, \mu_1) = & I^1(\tau_1, \mu_1) \tilde{b} + \frac{\tilde{c}(1 - 3g\mu_1\mu_0)}{\tilde{f}\mu_0\mu_1} \left[ \frac{\tilde{b}}{\exp(\tau_1/\mu_0)} - 1 \right] \\ & + \sum_{j=1}^2 S(\mu_1, \mu_{-j}) + \frac{\omega\phi(\mu_1, \mu_2)}{4\mu_1} \left\{ I^0(\tau_1, \mu_2) (\tilde{b} - \tilde{e}_2) \tilde{d}_2 \right. \\ & \left. + \frac{\tilde{c}(1 - 3g\mu_2\mu_0)}{\mu_0(1 - \omega) + \mu_2} \left[ \frac{\exp(\tilde{f}\tau_1) - 1}{\tilde{f}} - \frac{\tilde{b} - \tilde{e}_2}{\exp(\tau_1/\mu_0)} \tilde{d}_2 \right] \right\}, \end{aligned} \quad (10)$$

where

$$\begin{aligned} S(\mu_1, \mu_{-j}) = & \frac{\omega\phi(\mu_1, \mu_{-j})}{4\mu_1} \left\{ I^0(0, \mu_{-j}) \left( \frac{\tilde{b}}{\tilde{e}_{-j}} - 1 \right) \tilde{d}_{-j} \right. \\ & \left. + \frac{\tilde{c}(1 - 3g\mu_{-j}\mu_0)}{\mu_0(1 - \omega) + \mu_{-j}} \left[ \frac{\exp(\tilde{f}\tau_1) - 1}{\tilde{f}} - \left( \frac{\tilde{b}}{\tilde{e}_{-j}} - 1 \right) \tilde{d}_{-j} \right] \right\}, \end{aligned}$$

and

$$\begin{aligned} \tilde{b} &= \exp\{\tau_1[\omega\phi(\mu_1, \mu_1) - 4]/(4\mu_1)\}, \\ \tilde{c} &= \omega F_0 \mu_0 / (4\pi), \\ \tilde{d}_j &= 4\mu_1 \mu_j / \{4(1 - \omega)\mu_j + [\omega\phi(\mu_1, \mu_1) - 4]\mu_1\}, \\ \tilde{e}_j &= \exp[(\omega - 1)\tau_1/\mu_j], \\ \tilde{f} &= \{\mu_0[\omega\phi(\mu_1, \mu_1) - 4] - 4\mu_1\} / (4\mu_0\mu_1), \\ \phi(\mu_i, \mu_j) &= 1 + 3g\mu_i\mu_j, \\ (i, j) &= \pm 1, \pm 2. \end{aligned}$$

The value of  $I^0$  can be calculated by Eqs. (4) and (5) while  $I^1(\tau_1, \mu_1)$  is the boundary input computed from the previous layer. Similarly,  $I^1(0, \mu_2)$  can be obtained by changing  $\tilde{d}_2 \Rightarrow \tilde{d}_1$ ,  $\tilde{e}_2 \Rightarrow \tilde{e}_1$  and interchanging  $\mu_1 \Leftrightarrow \mu_2$  in Eq. (10) and its variable quantities. At last, the upward and downward fluxes are achieved as:

$$F^\uparrow(0) = 2\pi [a_1\mu_1 I^1(0, \mu_1) + a_2\mu_2 I^1(0, \mu_2)] \quad \text{and} \quad (11a)$$

$$\begin{aligned} F^\downarrow(\tau_1) = & 2\pi [a_1\mu_1 I^0(\tau_1, \mu_{-1}) + a_2\mu_2 I^0(\tau_1, \mu_{-2})] \\ & + \mu_0 \exp\left(-\frac{\tau_1}{\mu_0}\right) F_0. \end{aligned} \quad (11b)$$

And this  $\delta$ -four-stream scheme is named as  $\delta$ -4HSF.

### 3. Single column experiment

#### 3.1. Accuracy of the terrestrial schemes

The radiative transfer model used here is RRTMG\_LW, which contains 16 bands ranging from  $10 \text{ cm}^{-1}$  to  $3250 \text{ cm}^{-1}$ , including most greenhouse absorbers and several halocarbons. In this subsection, five TRT schemes are implanted in RRTMG\_LW to investigate their accuracy in an ideal atmosphere.

As single column experiment, the Mid-Latitude Summer atmospheric profile [37] is used here and divided into 200 layers with a resolution of 0.25 km from surface to 50 km. The benchmark results are calculated from the  $\delta$ -128-stream DOM scheme (D128S). Five sky conditions are considered: the clear sky, the skies with low cloud (positioned in 1.0-2.0 km with liquid water content LWC =  $0.22 \text{ g/m}^3$  and effective radius  $r_e = 5.89 \text{ }\mu\text{m}$ ), middle cloud (positioned in 4.0-5.0 km with LWC =  $0.28 \text{ g/m}^3$  and  $r_e = 6.2 \text{ }\mu\text{m}$ ), high cloud (positioned in 10.0-12.0 km with ice water content IWC =  $0.0048 \text{ g/m}^3$  and mean effective size  $D_e = 41.5 \text{ }\mu\text{m}$ ) and the sky containing above three types of clouds. The surface emissivity is set to 1. Due to the relation between heating rate and air density, a tiny net flux error can cause a huge error of heating rate at high altitude. And considering clouds and major synoptic processes exist only in troposphere, the height range analyzed in this section are constrained to 0-15 km. Also, it has to be noted that the solar radiation is excluded in this subsection.

Fig. 1 shows the comparison of heating rates in different sky conditions. The heating rate benchmarks displayed in the first column (Fig. 1a,e,i,m,q) are calculated from D128S and the corresponding absolute error profiles are computed from NS (second column),  $\delta$ -2DDA,  $\delta$ -2VIM (third column),  $\delta$ -4DDA and  $\delta$ -4VIM (fourth column). For the clear sky (Fig. 1a-d), all schemes have adequate performance that the maximum error is  $-0.12 \text{ K/day}$  using NS near the surface,  $0.09 \text{ K/day}$  using  $\delta$ -2DDA and  $\delta$ -2VIM, and  $0.03 \text{ K/day}$  using  $\delta$ -4DDA and  $\delta$ -4VIM. For heating rate errors in the cloudy skies (Fig. 1e-o), the maximum errors always appear around the cloud top and cloud base is where the second maximum errors occur. It is related to the large variations of heating rate at these two positions. In cloudy skies, the errors produced by NG scheme can be up to  $-3.44 \text{ K/day}$ ; the errors of the  $\delta$ -two-stream schemes (stand for  $\delta$ -2DDA and  $\delta$ -2VIM hereafter) are limited to  $1.52 \text{ K/day}$ , while  $\delta$ -2VIM is slightly more accurate than  $\delta$ -2DDA; the  $\delta$ -four-stream schemes (stand for  $\delta$ -4DDA and  $\delta$ -4VIM hereafter) achieve the best accuracy with the maximum error of  $-0.57 \text{ K/day}$ , while  $\delta$ -4DDA is slightly superior to  $\delta$ -4VIM.

#### 3.2. Accuracy of the overlap treatments

In this subsection, two overlap methods (WB and OB) for handling the region with solar and infrared spectra overlap are compared.

For WB, the solar irradiance in the overlap region is distributed into 1-15 bands ( $10$ - $2600 \text{ cm}^{-1}$ ) in RRTMG\_LW according to the solar irradiance dataset [31,32]. Note that the solar irradiance of band 16 ( $2600$ - $3250 \text{ cm}^{-1}$ ) is not included in the comparisons of WB and OB. Although band 16 also counts as overlap region, it is treated as an independent band in both RRTMG\_LW and RRTMG\_SW, which theoretically makes no difference to the accuracy of WB and OB. For 1-15 bands, the optical parameters (such as  $\tau$ ,  $\omega$  and  $g$ ) of SRT are shared with TRT. The total flux of WB is calculated as:

$$F_{WB} = F_{16}^{ter} + \sum_{j=1}^{15} (F_j^{sol} + F_j^{ter}), \quad (12)$$

where  $F_{WB}$  means the obtained flux using the schemes with the Whole Bands method, 16 and  $j$  is the band number of RRTMG, and

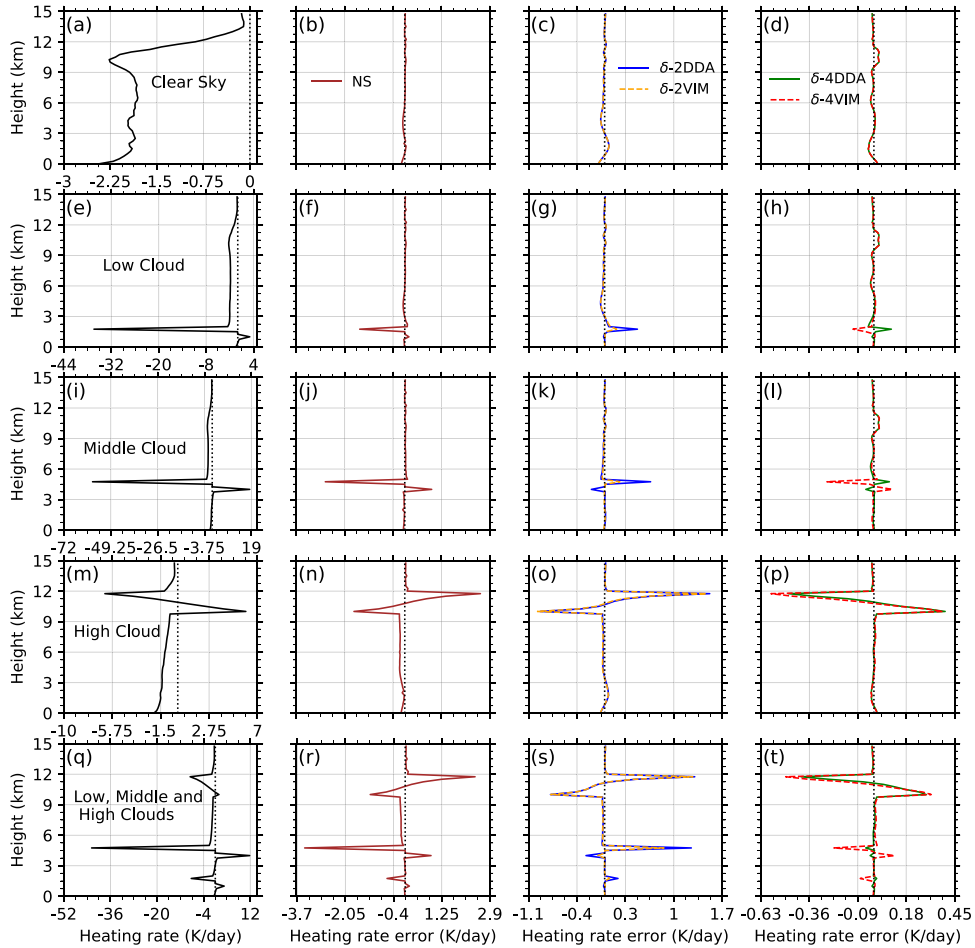


**Fig. 1.** The absolute heating rate errors (K/day) of NS schemes (second column), the  $\delta$ -two-stream schemes (third column) and the  $\delta$ -four-stream schemes (fourth column) against the benchmark results computed from D128S (first column) for the clear sky (first row); the skies with low cloud (second row), middle cloud (third row), high cloud (fourth row) and the sky containing all three cloud types (fifth row). The black dot lines represent the value of 0 (K/day).

$F_{29}^{sol}$  ( $F_j^{ter}$ ) stands for solar (terrestrial) part of flux. Note that when  $F_j^{ter}$  is calculated by  $\delta$ -2VIM ( $\delta$ -4VIM),  $F_{29}^{sol}$  is obtained by using the  $\delta$ -2HSF ( $\delta$ -4HSF) introduced in Section 2. And the terminology of the overall scheme is taken as “ $\delta$ -2VIM&HSF” (“ $\delta$ -4VIM&HSF”) in this work.

For OB,  $F_{29}^{sol}$  are calculated using RRTMG\_SW in the 820-2600  $\text{cm}^{-1}$  band (band 29, to be consistent with RRTMG\_SW), where the optical properties are the averaged results. The total downward solar flux at the TOA is the same in both WB and OB. The sum of solar and terrestrial fluxes of OB are calculated as:

$$F_{OB} = F_{29}^{sol} + \sum_{j=1}^{16} F_j^{ter}. \quad (13)$$

With the same atmosphere conditions used in Section 3.1, the heating rate errors of the four  $\delta$ -two/four-stream schemes using WB and OB are obtained against the benchmark results of D128S, which can address the incoming solar radiation in the infrared spectra accurately. The NS scheme is not considered in either WB or OB, because the errors of the NS scheme itself are much larger than errors introduced by different overlap methods.

In Fig. 2, benchmark heating rates are shown in the first column, and the  $\delta$ -two/four-stream schemes are compared in the second/third column respectively, while suffix ‘-WB’ (‘-OB’) stands for the Whole Bands method (the One Band method). As shown in Fig. 2e,f (Fig. 2h,i), the absolute value of maximum error calculated by  $\delta$ -2DDA-OB,  $\delta$ -2VIM&HSF-OB,  $\delta$ -4DDA-OB and  $\delta$ -4VIM&HSF-OB in the sky with low cloud (middle cloud) are 0.42, 0.46, 0.42 and

0.24 K/day (0.49, 0.52, 0.48 and -0.07 K/day) larger than their counterparts using WB. It is obvious that WB is more capable of dealing with the radiation in water cloud (low or middle cloud). For ice cloud (high cloud) displayed by Fig. 2k,l, situations are different between the  $\delta$ -two-stream and the  $\delta$ -four-stream schemes: the absolute value of maximum error calculated by  $\delta$ -2DDA-OB ( $\delta$ -2VIM&HSF-OB) is 0.21 (0.15) K/day larger than that of  $\delta$ -2DDA-WB ( $\delta$ -2VIM&HSF-WB), while that of  $\delta$ -4DDA-OB ( $\delta$ -4VIM&HSF-OB) is 0.03 (0.11) K/day smaller than that of  $\delta$ -4DDA-WB ( $\delta$ -4VIM&HSF-WB).

In general, being consistent with the result of Zhang et al. [33], the schemes using WB surpasses those using OB in handling the cloud radiation apart from a few exceptions.

## 4. Large-sample test

### 4.1. Accuracy of the terrestrial schemes

All results in Section 3 are based on single column experiment. And apparently, when only one reference atmospheric profile, a preset surface emissivity and fixed cloud distributions were used, the lack of representativeness is always a problem. Considering such limitation, further explorations are conducted with Large-sample test using more realistic atmosphere grid data (details can be found in 23) by combining MODIS data (MOD08\_M3; 38) and ERA-Interim reanalysis [39].

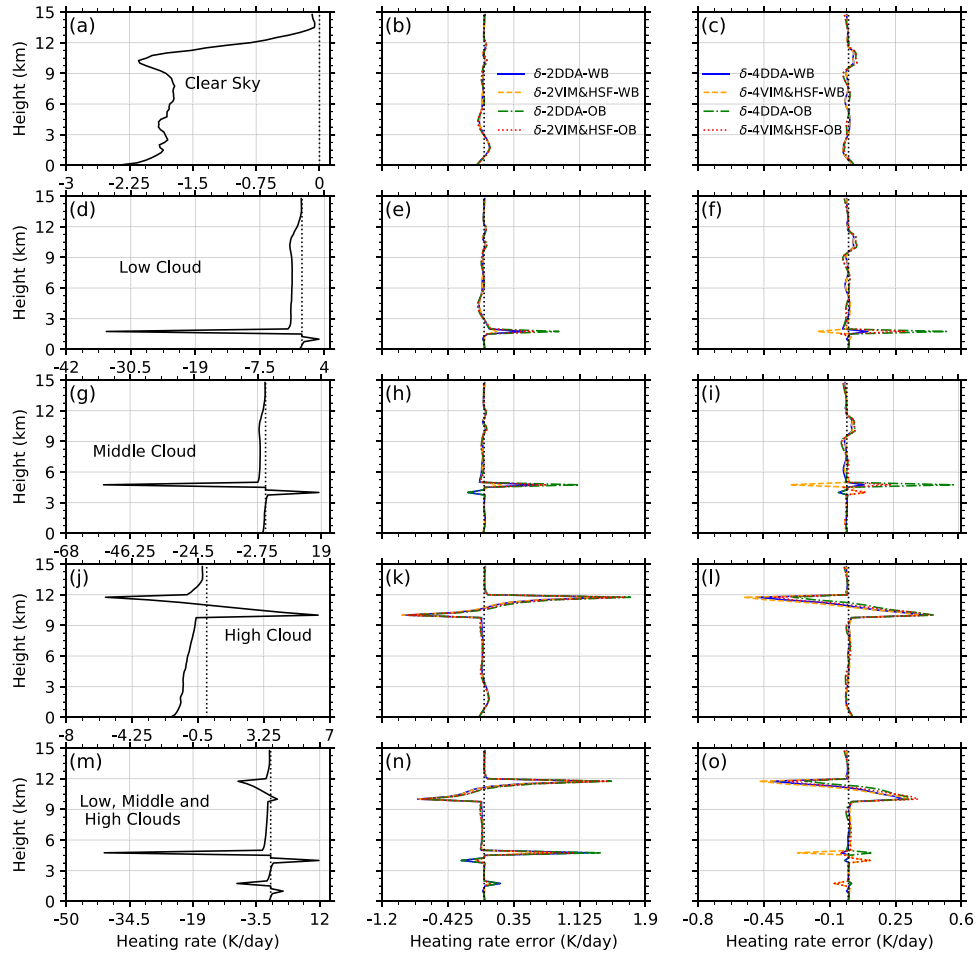


Fig. 2. Similar to Fig. 1, but without NS scheme, and suffix ‘-WB’ (‘-OB’) represents for the Whole Bands method (the One Band method).

Due to the enormous sample size, it is impossible to keep investigating the vertical properties of each grid. Therefore, in order to display the general characteristics of each column, a representative index needs to be established. As pointed out by Oreopoulos et al. [26], while longwave fluxes may be quite adequately simulated at the atmospheric column boundaries, net flux divergences within the atmosphere that determine heating (or cooling) rates may need further attention. By considering both radiative flux and heating rates, eventually, the net flux root mean squared error (RMSE, also known as standard error) of each column are calculated as follows:

$$RMSE(NF) = \sqrt{\frac{\sum_{k=1}^{NL} (NF_k - NF_k^{D128S})^2}{NL}}, \quad (14)$$

where NL is the total level number of each column,  $NF_k = F_k^\uparrow - F_k^\downarrow$  can be the net flux of any schemes at level k, and the order of  $F_k^\uparrow$  and  $F_k^\downarrow$  does not matter as long as it is consistent with that of  $NF_k^{D128S}$ , which is obtained in the same way as  $NF_k$  but the fluxes ( $F_k^\uparrow$  and  $F_k^\downarrow$ ) are calculated by D128S scheme.

Fig. 3a (Fig. 4a) shows the monthly averaged cloud fraction in January (July) 2018 and Fig. 3b-f (Fig. 4b-f) display the RMSE(NF) for NG,  $\delta$ -2DDA,  $\delta$ -2VIM,  $\delta$ -4DDA and  $\delta$ -4VIM schemes in the corresponding period. The different colormaps indicate the different value scales. Note that the blank areas are caused by the missing or fill data coming from MOD08\_M3. From Fig. 3 and Fig. 4, two evident tendencies can be found. Firstly, the general accuracy of the terrestrial schemes increases significantly in the order of

$NS < \delta$ -2DDA <  $\delta$ -2VIM <  $\delta$ -4DDA <  $\delta$ -4VIM. Secondly, the errors shown in Fig. 3b-f (Fig. 4b-f) are evidently related to the cloud fraction in Fig. 3a (Fig. 4a), which is consistent with common sense and the results gotten from Section 3.

However, there is also an unexpected phenomenon that can be seen in Fig. 3e,f (Fig. 4e,f). The accuracy of  $\delta$ -4DDA and  $\delta$ -4VIM may be poorer than that of  $\delta$ -2DDA and  $\delta$ -2VIM in the skies with less cloud. And it seems that  $\delta$ -4DDA and  $\delta$ -4VIM can handle the cloudy skies even better than those skies with less cloud. This phenomenon will be discussed again in the last paragraph of this subsection.

To further investigate the scheme accuracy, statistical graphs are drawn in Fig. 5. Fig. 5a displays the sample size distribution in different cloud fraction ranges ( $\pm 5\%$  of ticks in x-coordinate). The number of total samples in Fig 5a is 106494 consisting of 54096 samples from January 2018 and 52398 samples from July 2018. For Fig. 5b-f, the RMSE(NF) values of all samples are also sorted by cloud fraction ranges and shown by violin plots, of which the outer shape represents all possible values with thickness indicating how common and the inner marks illustrate a few statistical values. To be specific, the lower black crosses, middle yellow crosses, upper black crosses and red lines present the 10% quantiles, median, 90% quantiles and mean values respectively.

Two tendencies shown in Figs. 3 and 4 can be observed more clearly in Fig. 5. By comparing no matter the tick scales or the statistic marks in each colored bar of all schemes, the errors generally decrease in the order:  $NS > \delta$ -2DDA >  $\delta$ -2VIM >  $\delta$ -4DDA >  $\delta$ -4VIM, which is also confirmed by the statistics in

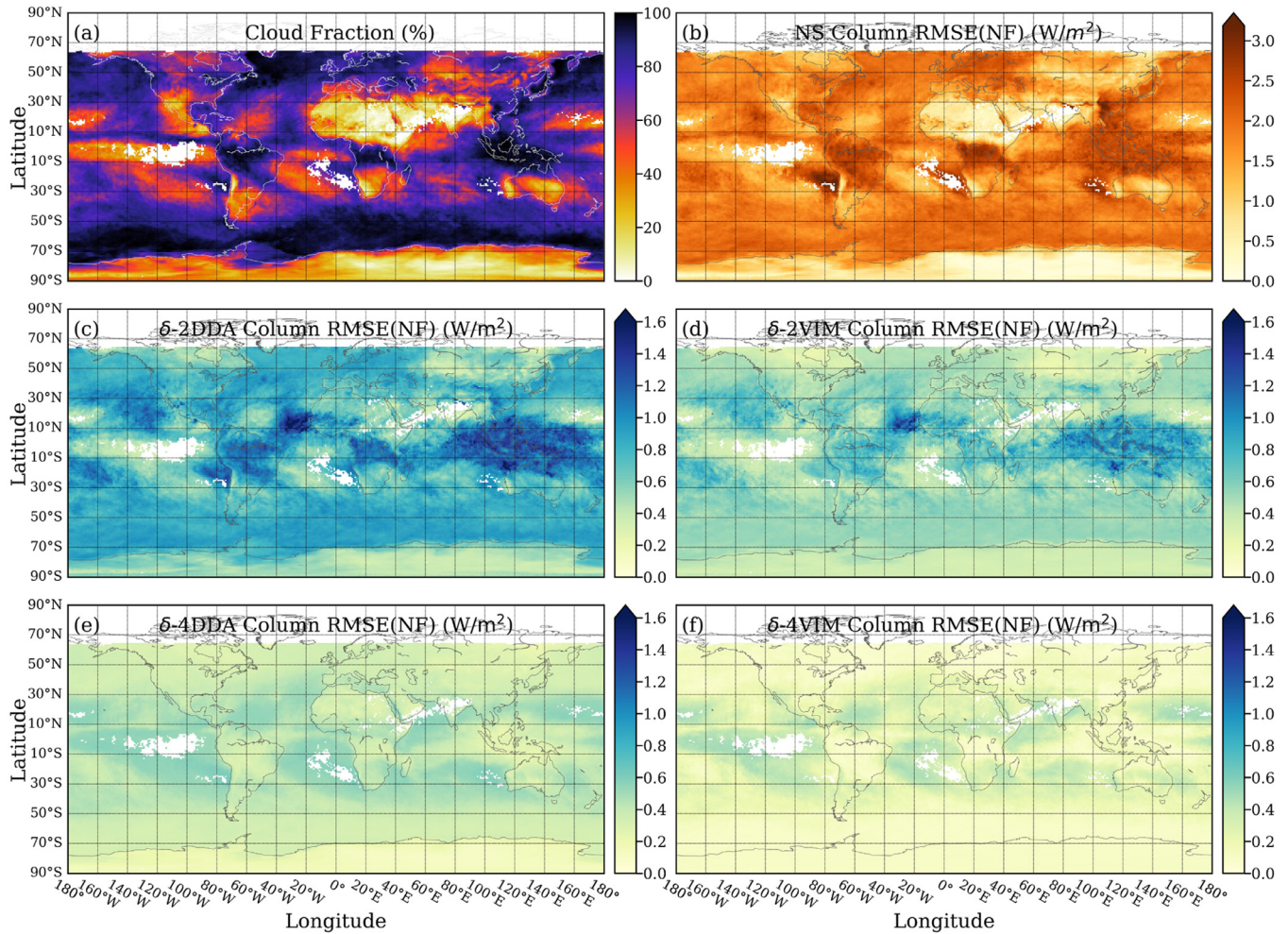


**Fig. 3.** (a) Cloud fraction (%) and the RMSE of column net fluxes ( $W/m^2$ ) for (b) NG, (c)  $\delta$ -2DDA, (d)  $\delta$ -2VIM, (e)  $\delta$ -4DDA and (f)  $\delta$ -4VIM in January 2018.

**Table 1**

RMSE(NF) statistics of all samples in January and July 2018 for the five schemes, including minimum, first quartile, median, third quartile, maximum, mean values and standard deviations.

Schemes	Minimum	25%	50%	75%	Maximum	Mean	S.D.
NS	0.11	1.45	1.80	2.02	4.81	1.70	0.50
$\delta$ -2DDA	0.21	0.66	0.80	0.90	2.58	0.79	0.21
$\delta$ -2VIM	0.12	0.45	0.51	0.58	2.24	0.54	0.15
$\delta$ -4DDA	0.10	0.34	0.39	0.46	0.62	0.39	0.10
$\delta$ -4VIM	0.03	0.11	0.17	0.29	0.75	0.21	0.11

**Table 1.** And their sensitivities of accuracy to cloud fraction are reduced in the same order. As shown in Fig. 5b,c, the RMSE(NF) mean values rise with the increase of cloud fraction, especially for NS scheme (Fig. 5b). And a wave shape begins to show up in the mean value tendency of Fig. 5c where the major trend of  $\delta$ -2VIM scheme is still the ascent though. However, when it comes to  $\delta$ -4DDA and  $\delta$ -4VIM in Fig. 5e,f, the line shape becomes wavier since their mean errors peak in the cloud fraction range of 40%-60%, and the errors of  $\delta$ -4VIM with cloud fraction over 70% even have the lowest mean values.

To hark back to the plausible supposition about the capabilities of  $\delta$ -4DDA and  $\delta$ -4VIM for handling the skies with less cloud, an unfavorable conclusion is obtained by observing Fig. 5. There is no distinct tendency that the  $\delta$ -two-stream schemes have better accuracy in the cloudy skies than the skies with less cloud (Fig. 5e,f). And the  $\delta$ -four-stream schemes have little inferiority in

dealing with the less cloudy skies compared to the  $\delta$ -two-stream schemes (Fig. 5c-f).

#### 4.2. Accuracy of the overlap treatments

The overlap methods are also examined by large-sample test. The RMSE(NF) of WB (OB) is obtained by substituting Eqs. (12) (13) into Eq. (14).

For the  $\delta$ -two-stream schemes, the RMSE(NF) values of WB and OB are presented in Fig. 6. By comparing  $\delta$ -2DDA or  $\delta$ -2VIM&HSF in different overlap treatments, though general tendencies of WB and OB change similarly with cloud fraction (Fig. 6), WB is superior to OB in accuracy in almost all aspects including the statistics (which can be confirmed in Table 2) and the distributions (which can also be reflected by the standard deviations listed in Table 2).

For the  $\delta$ -four-stream schemes using WB and OB (Fig. 7), the same nature that WB is superior to OB can be found. However, the relative amounts of errors introduced by overlap treatments have significant differences between the  $\delta$ -two-stream and the  $\delta$ -four-stream schemes. Taking the medium (50% quantiles) values in Table 2 as an example, the medium value of  $\delta$ -2DDA-OB is 1.42 times as large as that of  $\delta$ -2DDA-WB while this multiplier is magnified to 3 between  $\delta$ -4DDA-OB and  $\delta$ -4DDA-WB. Moreover, the multiplier in question is magnified with the rising of scheme accuracy:  $\delta$ -2DDA &  $\delta$ -2VIM&HSF <  $\delta$ -4DDA <  $\delta$ -4VIM&HSF, and this trend is not limited to the medium values. Furthermore, by calculating the absolute deviations between statis-

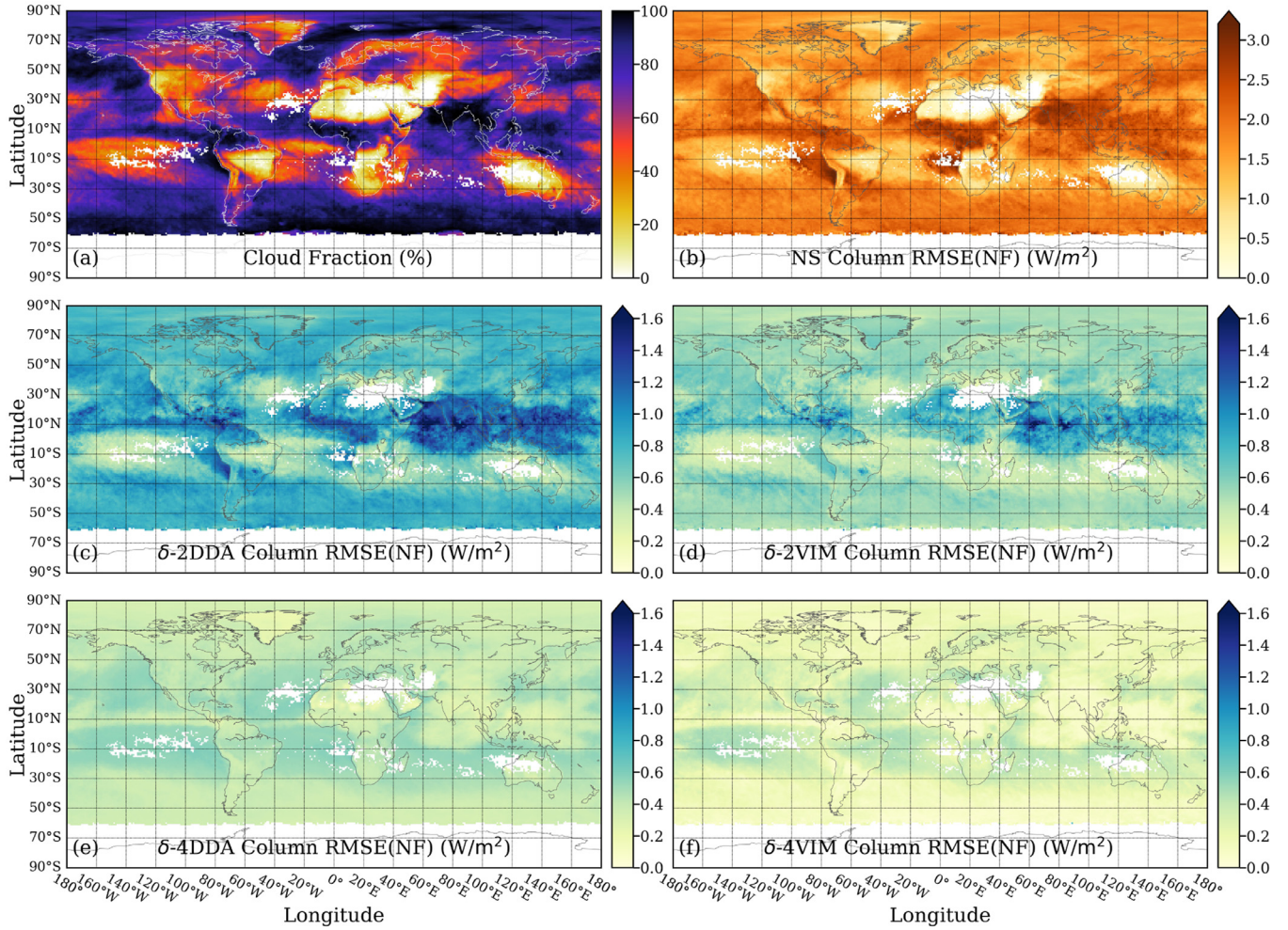


Fig. 4. The same as Fig. 3 but in July 2018.

**Table 2**  
Same as Table 1, but for the four terrestrial&solar schemes using WB and OB.

Schemes	Minimum	25%	50%	75%	Maximum	Mean	S.D.
Method 1: Whole Bands (WB)							
$\delta$ -2DDA-WB	0.21	0.64	0.78	0.87	2.55	0.77	0.20
$\delta$ -2VIM&HSF-WB	0.14	0.48	0.56	0.62	2.25	0.57	0.15
$\delta$ -4DDA-WB	0.10	0.34	0.39	0.46	0.62	0.39	0.10
$\delta$ -4VIM&HSF-WB	0.03	0.16	0.22	0.31	0.67	0.24	0.10
Method 2: One Band (OB)							
$\delta$ -2DDA-OB	0.26	0.95	1.11	1.29	2.94	1.11	0.28
$\delta$ -2VIM&HSF-OB	0.21	0.79	0.92	1.05	2.66	0.91	0.23
$\delta$ -4DDA-OB	0.20	0.64	0.85	0.97	1.30	0.80	0.23
$\delta$ -4VIM&HSF-OB	0.11	0.49	0.65	0.80	1.14	0.64	0.21

tics of WB and OB in Table 2, it can be found that the deviations of the  $\delta$ -four-stream schemes are higher than those of the  $\delta$ -two-stream schemes, and those of the  $\delta$ -two-stream (or  $\delta$ -four-stream) schemes are close to each other. For example, the mean value difference between  $\delta$ -4VIM&HSF-OB and  $\delta$ -4VIM&HSF-WB ( $0.40 \text{ W/m}^2$ ) is higher than that between  $\delta$ -2VIM&HSF-OB and  $\delta$ -2VIM&HSF-WB ( $0.34 \text{ W/m}^2$ ) but close to that between  $\delta$ -4DDA-OB and  $\delta$ -4DDA-WB ( $0.41 \text{ W/m}^2$ ). Hence, it is adequate to conjecture that the errors introduced by different overlap methods become more significant with the increase of the scheme accuracy.

Even though Figs 6, 7 and Table 2 can reflect the general errors of the solar and terrestrial flux, there is still positive-negative compensation (which stems from Eqs. 12 and 13) existing be-

tween them. This compensation might lead to the misjudgments of scheme accuracy. And since the terrestrial errors have been shown before (Section 4.1), the solar errors are yet to be discussed.

Both Fig. 8 and Table 3 display the RMSE(NF) statistics for the solar parts of  $F_{WB}$  and  $F_{OB}$  (Eqs. 12 and 13, which excluded all  $F^{ter}$ ). The errors are similar in the schemes using OB and significantly lower when using the schemes with WB. In Fig. 8, comparing the scales of RMSE(NF) among the schemes with WB,  $\delta$ -2DDA-WB and  $\delta$ -4DDA-WB have better accuracy, especially  $\delta$ -4DDA-WB. As for  $\delta$ -2HSF-WB and  $\delta$ -4HSF-WB, they are limited by their simple approximation of downward calculation (Eq. 2) and have lower accuracy. However, different from solar schemes using OB, the mean RMSE(NF) of all solar schemes with WB (Table 3) are much lower

## Terrestrial Errors in Infrared Region

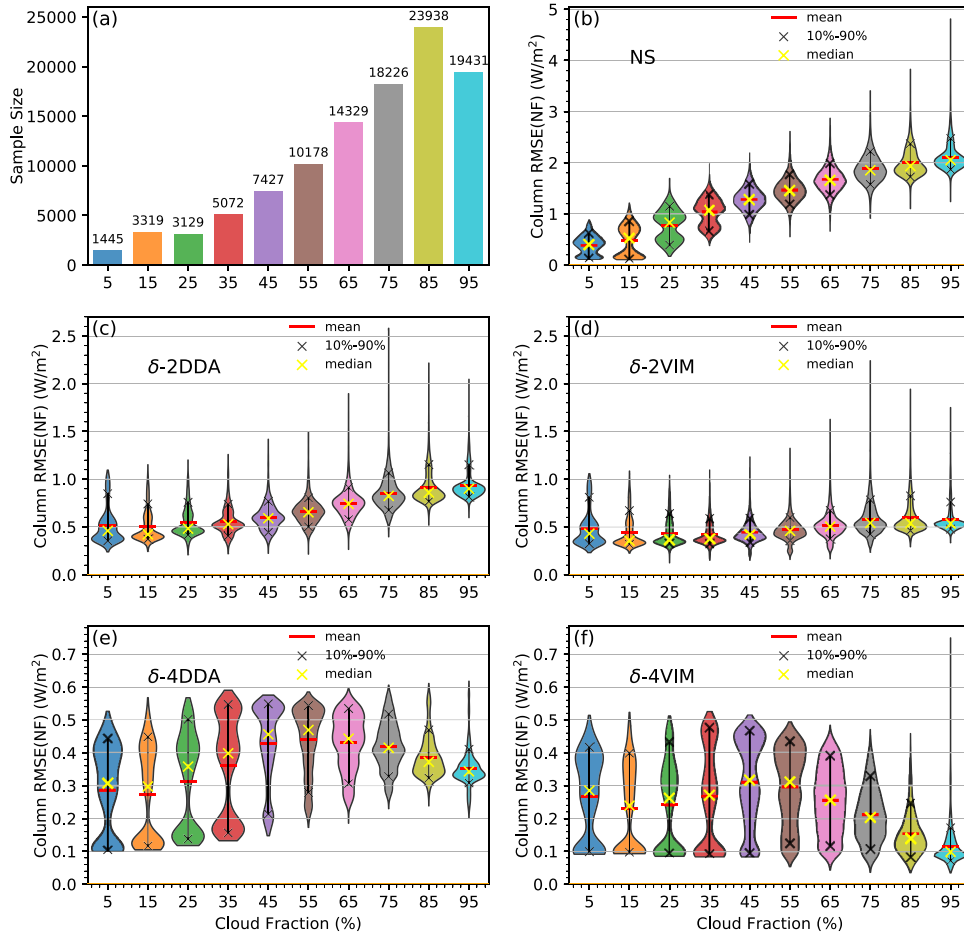


**Fig. 5.** Box plot (a) and violin plots (b-f) for all samples in January and July 2018 with the same scheme layout as Fig. 3. The numbers laid above the bars in plot (a) represent for sample sizes and each color stands for a cloud fraction range as well as a sample size.

**Table 3**

Same as Table 2, but for the solar radiation in the infrared region.

Schemes	Minimum	25%	50%	75%	Maximum	Mean	S.D.
Method 1: Whole Bands (WB)							
δ-2DDA-WB	0.00	0.02	0.03	0.04	0.07	0.03	0.01
δ-2HSF-WB	0.00	0.01	0.02	0.06	0.16	0.04	0.03
δ-4DDA-WB	0.00	0.00	0.00	0.00	0.01	0.00	0.00
δ-4HSF-WB	0.00	0.02	0.03	0.06	0.16	0.04	0.04
Method 2: One Band (OB)							
δ-2DDA-OB	0.07	0.26	0.46	0.53	0.72	0.41	0.15
δ-2HSF-OB	0.09	0.36	0.50	0.57	0.75	0.46	0.13
δ-4DDA-OB	0.06	0.31	0.49	0.56	0.75	0.44	0.15
δ-4HSF-OB	0.09	0.36	0.51	0.57	0.76	0.49	0.14

than those of terrestrial schemes (Table 1), which indicates that the solar schemes with WB only contribute the small parts to total radiation errors (Table 2). In that case, the major attention might be paid to the efficiency when choosing a solar scheme for infrared region.

Overall, WB is superior to OB in accuracy. And for the total radiation, the differences among the solar schemes using WB (or OB) are subtle.

### 5. Computational efficiency

The computational efficiency is always an essential criterion for radiation models. The timing discussed in this section is the CPU time obtained by using the FORTRAN intrinsic subroutine:

CPU\_TIME. Considering the precision of CPU\_TIME subroutine and to make the outcomes as stable as possible, each item shown in Table 4 is averaged from a loop of 10000 times of calculations. In Table 4, the computing time of five terrestrial schemes and the δ-two/four-stream schemes with WB and OB is obtained by Algorithm Only (which gets rid of processes like optical parameter preparation) or Radiation Model respectively to focus on the scheme performance or the application prospect. The '(&HSF)' in the first row of the table only valid with the Whole Bands or One Band case. Both results of Algorithm Only and Radiation Model are normalized to the terrestrial δ-2DDA scheme.

As shown in Table 4, the efficiency of NS looks incomparable, which is mainly due to the neglect of scattering and paid by the accuracy. And it is also because the NS timing here is more like

### $\delta$ -two-stream Terrestrial & Solar Errors in Infrared Region

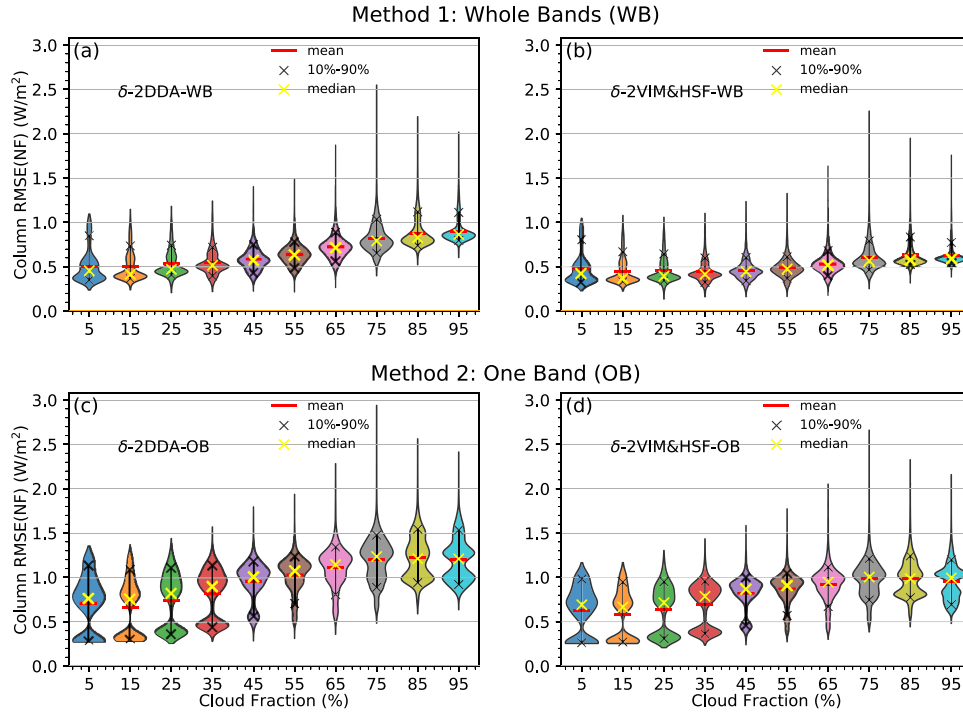


Fig. 6. Similar to Fig. 5, but for the terrestrial & solar results of  $\delta$ -two-stream schemes, and suffix '-WB' ('-OB') represent for the Whole Bands method (the One Band method).

### $\delta$ -four-stream Terrestrial & Solar Errors in Infrared Region

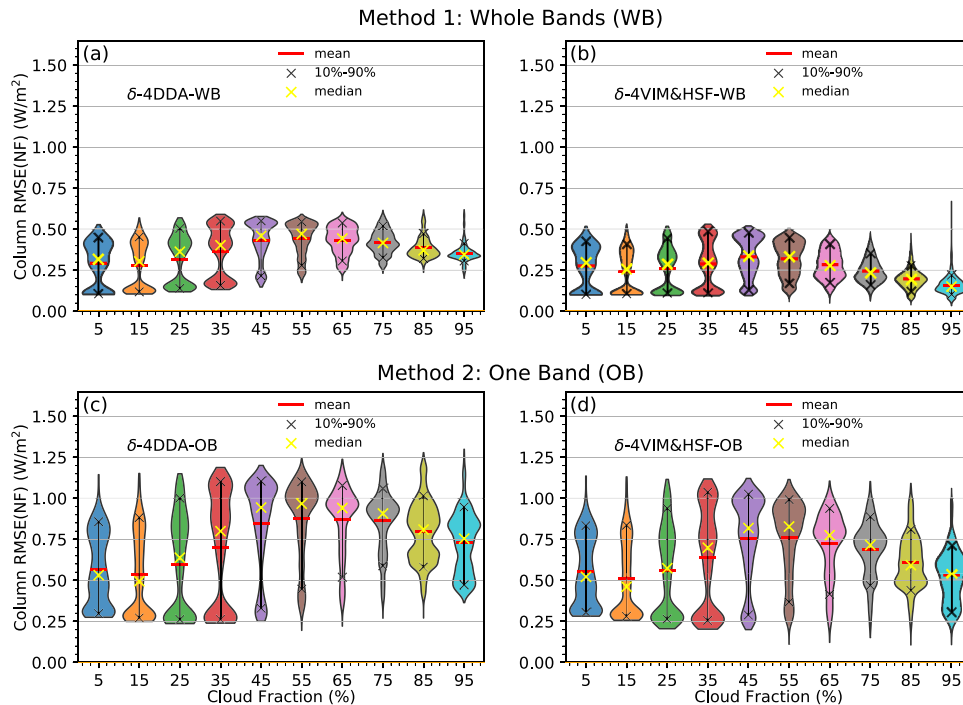
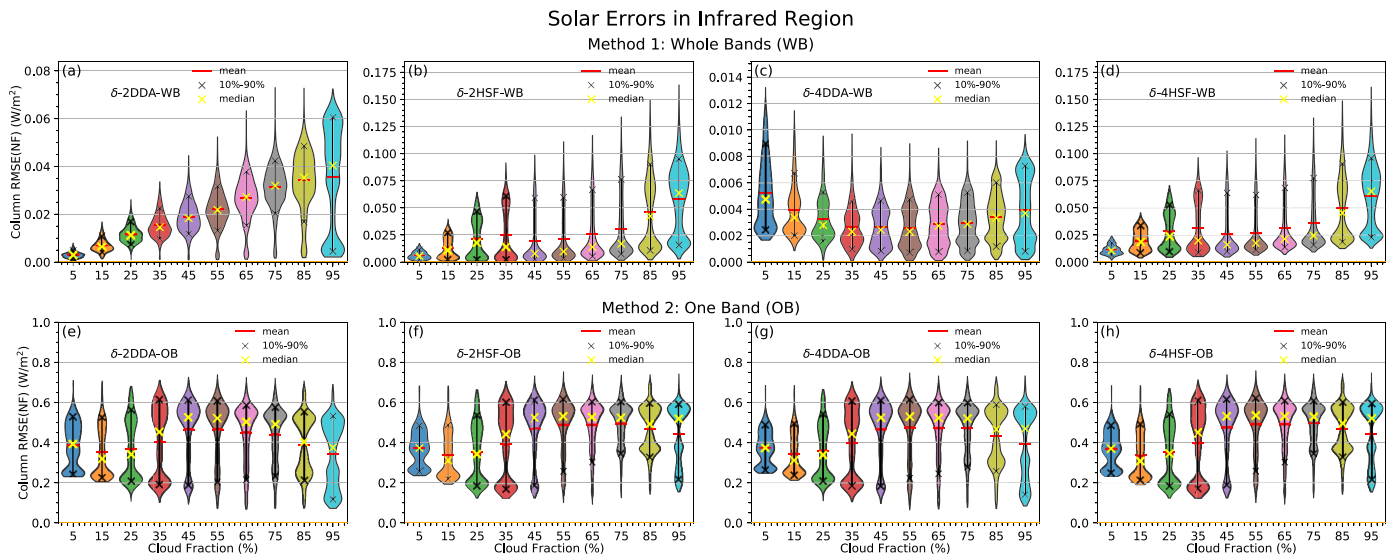


Fig. 7. The same as Fig. 6, but for  $\delta$ -four-stream schemes.

a reference standing for the efficiency of RRTMG\_LW original code, which adopts some advanced technologies like pre-computed look-up table for the Plank Function. Such technologies are not applied to any of the other schemes here since the code improvement is not the major aim of this work, which also means these schemes still have space to improve efficiency.

An interesting phenomenon can be found in Table 4 that the schemes with OB are more efficient than those with WB in the Algorithm Only scenario, but they are comparable to each other in the Radiation Model case. The reason is that the Algorithm Only scenario does not include the time consumed by optical parameter preparation, which is necessary for solar calculation in OB ( $F_{29}^{sol}$  in



**Fig. 8.** Similar to a combination of Figs. 6 and 7, but for the results of solar radiation. And note that the scales of the y-coordinate in the first row are not the same here.

**Table 4**

The timing of the radiative transfer calculations (normalized to the terrestrial  $\delta$ -2DDA scheme) with the terrestrial schemes and the schemes using WB and OB. The timing is calculated by Algorithm Only and Radiation Model.

Overlap treatments	NS	$\delta$ -2DDA	$\delta$ -2VIM (&HSF)	$\delta$ -4DDA	$\delta$ -4VIM (&HSF)
Algorithm Only					
Terrestrial Schemes	0.14	1.00	1.16	1.94	1.84
Whole Bands (Suffix '-WB')		1.20	1.25	3.17	3.27
One Band (Suffix '-OB')		1.10	1.28	2.28	2.12
Radiation Model					
Terrestrial Schemes	0.60	1.00	1.08	1.45	1.40
Whole Bands (Suffix '-WB')		1.09	1.12	2.02	2.07
One Band (Suffix '-OB')		1.53	1.62	2.11	2.02

Eq. (13)) but not needed for that in WB, where the optical parameters are shared by the solar and terrestrial calculations.

Generally, the efficiency of the  $\delta$ -two-stream (or  $\delta$ -four-stream) schemes are comparable to each other while the NS scheme is the most efficient. And for the schemes using WB in the Radiation Model case, the running time consumed by  $\delta$ -4DDA-WB ( $\delta$ -4VIM&HSF-WB) is about 1.85 times that of  $\delta$ -2DDA-WB ( $\delta$ -2VIM&HSF-WB).

## 6. Summary and conclusions

This paper presents the comparisons of performance for five TRT schemes and four  $\delta$ -two/four-stream schemes with two different overlap methods using RRTMG. And a simple scheme is established to deal with the solar radiation in the longwave region.

With a single column experiment, the heating rate errors are compared in Section 3. It is found that the maximum heating rate errors appear around the cloud top and the accuracy are increased in the order: NS <  $\delta$ -2DDA <  $\delta$ -2VIM <  $\delta$ -4VIM <  $\delta$ -4DDA. Moreover, the schemes with WB is broadly superior to those with OB in dealing with radiation under cloudy skies.

However, to detect the possible scheme behaviors in real applications, the single column experiment is far from enough. In Section 4, the large-sample test is conducted to compare the column RMSE(NF) of different TRT schemes and the schemes using different overlap methods. The errors are generally decreased in the sequence that NS >  $\delta$ -2DDA >  $\delta$ -2VIM >  $\delta$ -4DDA >  $\delta$ -4VIM, while their sensitivities of accuracy to cloud fraction are reduced in

the same order. In addition, WB overwhelms OB in accuracy, and such advantage is more significant in the  $\delta$ -four-stream schemes than that in the  $\delta$ -two-stream schemes.

Further exploration about computational efficiency is also presented. The NG scheme has matchless efficiency at the cost of accuracy. In the Radiation Model scenario, the schemes using WB run as fast as those using OB, and the time consumed by the schemes with WB varies as  $\delta$ -2DDA-WB  $\approx$   $\delta$ -2VIM&HSF-WB <  $\delta$ -4DDA-WB  $\approx$   $\delta$ -4VIM&HSF-WB, in which the running time of  $\delta$ -4DDA-WB ( $\delta$ -4VIM&HSF-WB) is about 1.85 times that of  $\delta$ -2DDA-WB ( $\delta$ -2VIM&HSF-WB).

Given that outstanding performance,  $\delta$ -4DDA-WB and  $\delta$ -4VIM&HSF-WB may deserve more promotions and extensive applications.

## Declaration of Competing Interests

The authors declare that they have no known competing financial interests or personal relationships that could have appeared to influence the work reported in this paper.

## CRediT authorship contribution statement

**Han Lin:** Methodology, Software, Formal analysis, Investigation, Resources, Writing - original draft, Data curation, Visualization. **Kun Wu:** Conceptualization, Software, Supervision, Writing - review & editing, Project administration, Funding acquisition. **Wenwen Li:** Writing - review & editing.

## Acknowledgement

The authors are grateful for the open-source codes of Rapid Radiative Transfer Model for General Circulation Models Applications (RRTMG) and the solar irradiance dataset from Atmospheric and Environmental Research, Inc. (AER, Inc.). This research work was supported by the National Key R&D Program of China (2018YFC1507002) and the National Natural Science Foundation of China (41675003 and 41675056).

## References

- [1] Chandrasekhar S. Radiative Transfer. Oxford University Press; 1950.
- [2] Liou KN. Analytic two-stream and four-stream solutions for radiative transfer. *J Atmos Sci* 1974;31(5):1473.
- [3] Coakley JAJ, Chylek P. The two-stream approximation in radiative transfer: including the angle of the incident radiation. *J Atmos Sci* 1975;32:409–18. doi:10.1175/1520-0469(1975)032<0409:TSAIR>2.0.CO;2.
- [4] Toon OB, Pollack JB, Sagan C. Physical properties of the particles composing the martian dust storm of 1971–1972. *Icarus* 1977;30(4):663–96. doi:10.1016/0019-1035(77)90088-4.
- [5] Wiscombe W. The delta-m method: Rapid yet accurate radiative flux calculations. *J Atmos Sci* 1977;34:1408–22. doi:10.1175/1520-0469(1977)034<1408:TDMRYA>2.0.CO;2.
- [6] Meador WE, Weaver WR. Two-stream approximations to radiative transfer in planetary atmospheres: A unified description of existing methods and a new improvement. *J Atmos Sci* 1988;37:630–43. doi:10.1175/1520-0469(1988)037<0630:TSATRT>2.0.CO;2.
- [7] Liou KN, Fu Q, Ackerman TP. A simple formulation of the delta-four-stream approximation for radiative transfer parameterizations. *J Atmos Sci* 1988;45:1940–7. doi:10.1175/1520-0469(1988)045<1940:ASFOTD>2.0.CO;2.
- [8] Toon OB, McKay CP, Ackerman TP. Rapid calculation of radiative heating rates and photodissociation rates in inhomogeneous multiple scattering atmospheres. *J Geophys Res* 1989;94:16287–301. doi:10.1029/JD094iD13p16287.
- [9] Shibata K, Uchiyama A. Accuracy of the delta-four-stream approximation in inhomogeneous scattering atmospheres. *J Meteor Soc Japan* 1992;70(6):1097–109. doi:10.2151/jmsj1965.70.6.1097.
- [10] Li J, Ramaswamy V. Four-stream spherical harmonic expansion approximation for solar radiative transfer. *J Atmos Sci* 1996;53:1174–86. doi:10.1175/1520-0469(1996)053<1174:FSSHEA>2.0.CO;2.
- [11] Fu Q, Liou KN, Cribb MC, Charlack TP, Grossman A. Multiple scattering parameterization in thermal infrared radiative transfer. *J Atmos Sci* 1997;54:2799–812. doi:10.1175/1520-0469(1997)054<2799:MSPITI>2.0.CO;2.
- [12] Van Oss RF, Spurr RJ. Fast and accurate 4 and 6 stream linearized discrete ordinate radiative transfer models for ozone profile retrieval. *J Quant Spectrosc Radiat Transfer* 2002;75:177–220. doi:10.1016/S0022-4073(01)00246-1.
- [13] Zhang H, Zhang F, Fu Q, Shen Z, Lu P. Two- and four-stream combination approximations for computation of diffuse actinic fluxes. *J Atmos Sci* 2010;67:3238–52. doi:10.1175/2010JAS3370.1.
- [14] Lin L, Fu Q, Zhang H, Su J, Yang Q, Sun Z. Upward mass fluxes in tropical upper troposphere and lower stratosphere derived from radiative transfer calculations. *J Quant Spectrosc Radiat Transfer* 2013;117:114–22. doi:10.1016/j.jqsrt.2012.11.016.
- [15] Zhang F, Li J, Zhang H, Ma L, Zhou X. On the relationship between direct and diffuse radiation. *J Quant Spectrosc Radiat Transfer* 2013;115:60–5. doi:10.1016/j.jqsrt.2012.09.009.
- [16] Zhang F, Shen Z, Li J, Zhou X, Ma L. Analytical delta-four-stream doublingadding method for radiative transfer parameterizations. *J Atmos Sci* 2013;70(3):794–808. doi:10.1175/JAS-D-12-0122.1.
- [17] Zhang F, Li J. Doublingadding method for delta-four-stream spherical harmonic expansion approximation in radiative transfer parameterization. *J Atmos Sci* 2013;70(10):3084–101. doi:10.1175/JAS-D-12-0334.1.
- [18] Zhang H, Wang Z, Zhang F, Jing X. Impact of four-stream radiative transfer algorithm on aerosol direct radiative effect and forcing. *Int J Climatol* 2015;35(14):4318–28. doi:10.1002/joc.4289.
- [19] Wang B. A unified formulation of radiative transfer in plane-parallel atmospheres based on general decomposition of radiance. part i: The theory. *J Atmos Sci* 2017;74(12):4139–51. doi:10.1175/JAS-D-16-0272.1.
- [20] Zhang F, Shi Y-N, Li J, Wu K, Iwabuchi H. Variational iteration method for infrared radiative transfer in a scattering medium. *J Atmos Sci* 2017;74(2):419–30. doi:10.1175/JAS-D-16-0172.1.
- [21] Shi Y-N, Zhang F, Yan J-R, Iwabuchi H, Wang Z. The standard perturbation method for infrared radiative transfer in a vertically internally inhomogeneous scattering medium. *J Quant Spectrosc Radiat Transfer* 2018;213:149–58. doi:10.1016/j.jqsrt.2018.03.025.
- [22] Shi Y-N, Zhang F, Chan KL, Trautmann T, Li J. Multi-layer solar radiative transfer considering the vertical variation of inherent microphysical properties of clouds. *Opt Express* 2019;27(20):A1569–90. doi:10.1364/OE.27.0A1569.
- [23] Lin H, Zhang F, Wu K, Xu J. Comparisons of  $\delta$ -two-stream and  $\delta$ -four-stream radiative transfer schemes in rrtmg for solar spectra. *SOLA* 2019;15:87–93. doi:10.2151/sola.2019-017.
- [24] Li J. Accounting for unresolved clouds in a 1d infrared radiative transfer model. part i: Solution for radiative transfer, including cloud scattering and overlap. *J Atmos Sci* 2002;59:3302–20. doi:10.1175/1520-0469(2002)059<3302:AFUCIA>2.0.CO;2.
- [25] Costa SMS, Shine KP. An estimate of the global impact of multiple scattering by clouds on outgoing long-wave radiation. *Q J R Meteor Soc* 2006;132(616):885–95. doi:10.1256/qj.05.169.
- [26] Oreopoulos L, Mlawer E, Delamere J, Shipper T, et al. The continual intercomparison of radiation codes: Results from phase i. *J Geophys Res* 2012;117(D6). doi:10.1029/2011JD016821.
- [27] Zhang F, Wu K, Li J, Yang Q, Zhao JQ, Li J. Analytical infrared delta-four-stream adding method from invariance principle. *J Atmos Sci* 2016;73(10):4171–88. doi:10.1175/JAS-D-15-0317.1.
- [28] Wu K, Zhang F, Min J, Yu QR, Wang XY, Ma L. Adding method of delta-four-stream spherical harmonic expansion approximation for infrared radiative transfer parameterization. *Infrared Phys Technol* 2016;78:254–62. doi:10.1016/j.infrared.2016.08.001.
- [29] Wang B. A unified formulation of radiative transfer in plane-parallel atmospheres based on general decomposition of radiance. part ii: An exemplifying application to the hemispherical harmonics method with four components. *J Atmos Sci* 2017;74(12):4153–76. doi:10.1175/JAS-D-17-0024.1.
- [30] Clough S, Shephard M, Mlawer E, Delamere J, Iacono M, Cady-Pereira K, et al. Atmospheric radiative transfer modeling: a summary of the aer codes. *J Quant Spectrosc Radiat Transfer* 2005;91(2):233–44. doi:10.1016/j.jqsrt.2004.05.058.
- [31] Lean JL, Woods TN. Solar spectral irradiance: measurements and models. Cambridge University Press; 2010. p. 269–98.
- [32] Coddington O, Lean J, Pilewskie P, Snow M, Lindholm D. A solar irradiance climate data record. *Bull Amer Meteor Soc* 2016;97(7):1265–82. doi:10.1175/BAMS-D-14-00265.1.
- [33] Zhang F, Wu K, Li J, Zhang H, Hu S. Radiative transfer in the region with solar and infrared spectra overlap. *J Quant Spectrosc Radiat Transfer* 2018;219:366–78. doi:10.1016/j.jqsrt.2018.08.025.
- [34] Li J, Fu Q. Absorption approximation with scattering effect for infrared radiation. *J Atmos Sci* 2000;57:2905–14. doi:10.1175/1520-0469(2000)057<2905:AAWSEF>2.0.CO;2.
- [35] Fu Q. Parameterization of radiative processes in vertically nonhomogeneous multiple scattering atmospheres. University of Utah; 1991.
- [36] Sykes JB. Approximate integration of the equation of transfer. *Mon Not R Astron Soc* 1951;111:377–86. doi:10.1093/mnras/111.4.377.
- [37] Anderson GP, Clough SA, Kneizys F, Chetwynd JH, Shettle EP. Aflg atmospheric constituent profiles (0.120 km). Tech. Rep. Air Force Geophys. Lab., Hanscom Air Force Base, Bedford, Mass; 1986.
- [38] Platnick S, King M, Meyer K, Wind G, Amarasinghe N, Marchant B, et al. Modis atmosphere l3 monthly product. NASA MODIS Adaptive Processing System, Goddard Space Flight Center, USA; 2015. doi:10.5067/MODIS/MOD08\_M3.006.
- [39] Dee DP, Uppala S, Simmons A, Berrisford P, Poli P, Kobayashi S, et al. The era-interim reanalysis: Configuration and performance of the data assimilation system. *Q J R Meteor Soc* 2011;137(656):553–97. doi:10.1002/qj.828.
- [40] Xue D, Zhang F, Shi Y-N, Iwabuchi H, Li J, Hu S, et al. The  $\delta$ -six-stream spherical harmonic expansion adding method for solar radiative transfer. *J Quant Spectrosc Radiat Transfer* 2020;243:106818. doi:10.1016/j.jqsrt.2019.106818.